Taylor & Francis
Taylor & Francis Group

Low intensity pulsed ultrasound ameliorates Adriamycin-induced chronic renal injury by inhibiting ferroptosis

Zhi-Qiang Ouyang[a]*, Li-shi Shao[b]*, Wei-peng Wang[c]*, Teng-fei Ke[d], Dong Chen[e], Guang-rong Zheng[a], Xi-rui Duan[d], Ji-xiang Chu[d], Yu Zhu[d], Lu Yang[d], Hai-yan Shan[a], Lin Huang[c] and Cheng-de Liao [ID][a]

[a]Department of Radiology, Yan` an Hospital of Kunming City (Yanan Hospital Affiliated to Kunming Medical University), Kunming, People's Republic of China; [b]Department of Radiology, The Second Affiliated Hospital of Kunming Medical University, Kunming, People's Republic of China; [c]School of Electronic Science and Engineering, University of Electronic Science and Technology of China, Chengdu, People's Republic of China; [d]Department of Radiology, Yunnan Cancer Hospital (The Third Affiliated Hospital of Kunming Medical University), Kunming, People's Republic of China; [e]Department of Ultrasound, Yunnan Cancer Hospital (The Third Affiliated Hospital of Kunming Medical University), Kunming, People's Republic of China

ABSTRACT

Objective: It is very important to develop a new therapeutic strategy to cope with the increasing morbidity and mortality of chronic kidney disease (CKD). As a kind of physical therapy, low intensity pulsed ultrasound (LIPUS) has remarkable anti-inflammatory and repair-promoting effects and is expected to become a new therapeutic method for CKD. This study aims to clarify the treatment effect of LIPUS on CKD-related renal inflammation and fibrosis, and to further explore the potential signal network of LIPUS treatment for ameliorating chronic renal injury.

Methods: A rat model simulating the progress of CKD was established by twice tail-vein injection of Adriamycin (ADR). Under anesthesia, bilateral kidneys of CKD rats were continuously stimulated by LIPUS for four weeks. The parameters of LIPUS were 1.0 MHz, 60 mW/cm^2, 50% duty cycle and 20 min/d.

Results: LIPUS treatment effectively inhibited ADR-induced renal inflammation and fibrosis, and improved CKD-related to oxidative stress and ferroptosis. In addition, the therapeutic effect of LIPUS is closely related to the regulation of TGF-β_1/Smad and Nrf2/keap1/HO-1 signalling pathways.

Discussion: This study provides a new direction for further mechanism research and lays an important foundation for clinical trials.

1. Introduction

Chronic kidney disease (CKD) is known to be a major public health problem, which plagues about 9.1% of the global population [1]. According to conservative estimates, more than 1 million people die every year from CKD and its complications [1,2]. Pathologically, repeated renal inflammation is an important inducement for the development of renal fibrosis [3]. In addition, regardless of the primary disease, renal fibrosis is always the most common pathological manifestation in end-stage renal disease (ESRD), and it is the main cause of further inflammation and progressive renal failure [4]. Therefore, inhibition of renal inflammation and fibrosis may be the key to protect renal function in CKD patients.

Low intensity pulsed ultrasound (LIPUS) is a kind of ultrasound wave with a frequency of 1–3 MHz and an intensity of < 1 W/cm^2, which can transmit low-frequency and low-intensity sound signals as acoustic pressure waves to tissue [5]. Compared with traditional drug therapy, LIPUS has the advantages of non-invasive, tolerable, and minimal side effects. Its therapeutic efficacy is mainly attributed to non-thermal effects, such as cavitation, acoustic streaming and acoustic radiation force [6]. After decades of research, the efficacy of LIPUS in inhibiting local inflammation [5,7] and promoting tissue repair [8,9] has been gradually developed. Importantly, LIPUS stimulation in vitro is consistent with the key to CKD treatment. Aibara et al. provided the first evidence that suitable LIPUS stimulation could ameliorate renal inflammation and fibrosis in experimental hypertension and diabetes-related CKD [10]. Moreover, a recent study found that LIPUS stimulation can alleviate the progress of CKD by inhibiting renal fibrosis, restoring antioxidant enzymes, weakening the aging of renal failure and reducing the level of uraemic toxin indophenol sulphate [11]. However, little is known about the exact mechanism by which LIPUS exerts protective effects on CKD.

For a long time, preventing cell death has been considered as an important target to inhibit renal fibrosis and improve renal function injury [12]. At present, the mainstream view holds that the forms of cell death mainly include apoptosis, necroptosis, pyroptosis, autophagy and ferroptosis [13]. Particularly, ferroptosis as a newly identified type of cell death, which is characterised by intracellular iron accumulation and lipid peroxidation, and is regulated by various metabolic and signalling pathways, including system Xc− (cysteine/glutamate antiporter), glutathione peroxidase 4 (GPX4), iron

homeostasis and reactive oxygen species (ROS) signalling [14,15]. Recent studies revealed that ferroptosis plays a critical role in different CKD syndromes [16–18]. In other words, long-term chronic kidney injury is dominated by renal inflammation and fibrosis, which could be defined by ferroptosis in CKD [19]. Therefore, investigating the regulation of ferroptosis in CKD is the prerequisite for developing new targets and therapeutic strategies. LIPUS has been proved to inhibit renal inflammation and fibrosis by reducing oxidative damage [11], but whether it involves ferroptosis signal transduction needs further investigation.

In this study, we first investigated the inhibitory effect of LIPUS on renal inflammation and fibrosis in the CKD rat model which was induced by Adriamycin (ADR). Because this rodent mode is a stable and well-established model for determining expression changes of cell death, inflammation, oxidative stress injury and fibrosis symptoms in abnormal kidneys [20]. Subsequently, we preliminarily explored the potential mechanism of LIPUS to regulate the CKD-related ferroptosis signalling. Hope to provide new direction and pre-clinical basis for the clinical treatment of CKD.

2. Materials and methods

2.1. Ethics statement

This study was approved by the Ethics Committee of Kunming Medical University (approval number: Kmmu20220330) and was performed in accordance with the ethical standards laid down in the 1964 Declaration of Helsinki and its later amendments. All animal experiments followed the National Institutes of Health (NIH) guidelines to ensure the welfare of animals and reduce their suffering.

2.2. Animal and ADR-induced CKD model

Male Sprague Dawley (SD) rats (6–8 weeks, 180–220 g) used in this study were purchased from the Experimental Animal Centre of Kunming Medical University (SPF, license number SYXK (Dian) k 2020-0006), and all animal experiments were conducted in this centre. All rats were housed in cages at room temperature (22 ± 2℃), with 12 h light/dark cycles (lights were turned on at 7:00 am). During the experiment, food and water were sufficient and freely available, the padding was replaced every 3 days. The rats were randomly divided into Control group, CKD group and CKD + LIPUS group (n = 6 per group). To induce CKD, the rats were fed adaptively for one week, and then received twice tail vein injections of ADR solution (Sigma Aldridge, USA), with a two-weeks interval. The concentration and injection dose of ADR solution were 2 mg/ml and 4 mg/kg, respectively [21]. The Control group rats were injected with an equal volume of physiological saline at the same time. Four weeks after injection of ADR or physiological saline, all rats were euthanised.

2.3. LIPUS treatment

The LIPUS device consists of an arbitrary waveform function generator (SDG1022X, Siglent, Shenzhen, China), an oscilloscope (TDS2022B, Tektronix, Shanghai, China) and ultrasound transducers (Φ = 3 cm). Among them, the ultrasound transducers were specially manufactured and tested by the Academy of Electronics and Engineering (the University of Electronic Science and Technology of China, Chengdu, China) for rat in vitro experiments. Before LIPUS stimulation, hair on the back of each rat was removed, the positions of bilateral kidneys were determined and marked by ultrasound imaging. Then, the ultrasound transducers were placed over the back marker with an ultrasonic gel pad (Mibo, Mp-A, Shenzhen, China) in between. Rats in the CKD + LIPUS group were stimulated by LIPUS for 20 min every 24 h, treatment duration was four weeks. During this period, isoflurane (R510-22-10, RWD, Shenzhen, China) was produced by the gas anaesthesia machine (MSSVAP01, MSS, Keighley, England) to keep rats under anaesthesia. According to previous studies [10,11] and our preliminary experimental results, the parameters of LIPUS are set as follows: intensity of 60 mW/cm^2 with a 50% duty cycle, and pulse frequency of 1.0 MHz with 1 kHz repetition rate. As for the Control group and the CKD group, which received the same treatments except LIPUS stimulation.

2.4. Renal function assay

Rats were individually kept in metabolic cages for 24 h, and urine samples were collected at day 0, 21 and 42. Urinary albumin was measured using a rat albumin ELISA quantitation kit (C035-2, Jiancheng Bioengineering Institute, Nanjing, China) according to the manufacturer's protocol. A fully automatic biochemical analyser (Chemray 800, Rayto, Shenzhen, China) was used to measure the serum creatinine (Scr) and blood urea nitrogen (BUN) levels.

2.5. Ultrasonic elastography

A high-end colour Doppler ultrasound system (Resona R9, Mindray, Shenzhen, China) with a 3–11 MHz probe was used to measure kidney hardness representing the degree of renal fibrosis in rats. Briefly, in the conventional imaging mode, the probe was perpendicular to unilateral kidney of rat and locked its position. Next, an elastic sampling frame was placed to surround the whole kidney in the elastic imaging mode (for accurate imaging, it is necessary to ensure that the kidney was in the center). The index value of pressure should be controlled between 2 and 3 through a vibration test. Finally, the dual real-time imaging function was used to capture both conventional ultrasound images and elastic images. The bilateral kidneys of each rat were measured three times repeatedly.

2.6. Histopathological assay

Kidney tissue was fixed with 4% paraformaldehyde for 24 h, dehydrated with 7% sucrose for three times, embedded in paraffin, and then cut into 4 μm sections and taken on slides. The prepared slides were deparaffinised twice in xylene and rehydrated in gradient ethanol, and then stained separately with haematoxylin–eosin (H&E), periodic acid Schiff (PAS), Masson's trichrome and iron staining. Sections were scanned by using an optical microscope (Aperio VERSA, Laica, Shanghai, China). Then, 15 fields per slice were randomly selected analysis. According to the pathological changes of cortical areas in H&E staining, the renal injury score was evaluated, including renal tubular dilatation, necrotic tubular cells, glomerular tuff, sclerosis, and inflammatory cell infiltration. Abnormal areas were

evaluated using a blind test with scores of 0 = normal; 1 = mild injury (<25%, abnormal pathology injury); 2 = moderate injury (25–50%); 3 = severe injury (50–75%); and 4 = large area injury (>75%). For Masson's trichrome and iron staining, the areas of fibrosis and iron deposition were quantified as the average value of each slice by Image J software (http://rsb.info.nih.gov/ij).

2.7. Transmission electron microscopy

Fresh kidney tissue was immediately fixed with 2.5% glutaraldehyde (G1102, Serviocebio, Wuhan, China) for 3 h at 4℃. Subsequently, it was rinsed with 1× phosphate buffer saline (PBS) for three times. Postfixed in 1% aqueous osmium tetroxide for 2 h at room temperature, dehydrated in gradual ethanol (50%–100%), embedded in epoxy resin monomer and cured for 48 h at 60℃. Ultra-thin slices of 50 nm were cut and stained with uranyl acetate and lead citrate. Three samples were selected for each group and examined by transmission electron microscope (HT7700-SS; HITACHI, Tokyo, Japan).

2.8. Inflammatory factors and ferroptosis-related indicators assay

The contents of interleukin-1β (IL-1β) and interleukin-6 (IL-6) in renal cortex were measured using the enzyme-linked immunosorbent assay (ELISA) kits (DG20049D and DG94490Q, Dogesce, Beijing, China). The levels or activities of Fe^{2+}, lipid peroxide (LPO), superoxide anionic (O_2^-), malondialdehyde (MDA), total superoxide dismutase (T-SOD), glutathione (GSH) and glutathione peroxidase (GSH-Px) were measured using the colorimetric assay kits (E-BC-K773-M, E-BC-K176-M, E-BC-K001-M, E-BC-K025-M, E-BC-K020-M, E-BC-K030-M and E-BC-K096-M, Elabscience, Wuhan, China). All tests and analyses were performed according to the manufacturer's instructions.

2.9. TUNEL and ROS assay

Kidney cryosections were cut into 10 μm sections on a cryostat. Next, a reagent was added to incubate kidney tissue for 5 min to quench spontaneous fluorescence. After rinsing in tap water for 10 min, TUNEL staining solution (G1501, Serviocebio, Wuhan, China) and ROS staining solution (G1723, Serviocebio, Wuhan, China) were added to the marked area respectively. Then it was incubated at 37℃ for 30 min and placed in a dark. The slices were scanned with optical microscope and quantified with Image J software.

2.10. Real-Time quantitative polymerase chain reaction (RT-qPCR)

The expression of key genes was detected using RT-qPCR. Total RNA was extracted from kidney tissues by TRIzol reagent (G3013, Serviocebio, Wuhan, China). Complementary DNA (cDNA) was synthesised by the reverse transcription kit (G3330, Serviocebio, Wuhan, China). Finally, qPCR was carried out by the CFX Connect system (Hercules, Bio-Rad Laboratories, Inc., CA, USA) using 2 × SYBR Green qPCR Master Mix (G3320, Serviocebio, Wuhan, China). Genes expression levels were normalised to the house-keeping

Table 1. Specific primers for RT-qPCR.

Gene	Sequence (5′–3′)
IL-1β	Forward: CCTATGTCTTGCCCGTGGAG
	Reverse: CACACACTAGCAGGTCGTCA
IL-6	Forward: CCACCCACAACAGACCAGTA
	Reverse: GGAACTCCAGAAGACCAGAGC
Fibronectin	Forward: GATGAGCTTCCCCAACTGGT
	Reverse: ACTGGGTTGTTGGTGGGATG
α-SMA	Forward: AGACCCTCTTCCAGCCATCT
	Reverse: CCCCGAGAGGACGTTGTTAG
TGF-β₁	Forward: CACTCCCGTGGCTTCTAGTG
	Reverse: CTGGCGAGCCTTAGTTTGGA
GPX4	Forward: GATGGAGCCCATTCCTGAACC
	Reverse: CCCTGTACTTATCCAGGCAGA
Nrf2	Forward: TCTTGGAGTAAGTCGAGAAGTGT
	Reverse: GTTGAAACTGAGCGAAAAAGGC
β-actin	Forward: CGTAGCCATCCAGGCTGTGTT
	Reverse: AATGTCACGCACGATTTCCCT

α-SMA: α-smooth muscle actin; GPX4: glutathione peroxidase 4; IL-1β: interleukin-1β; IL-6: interleukin-6; Nrf2: nuclear factor erythroid 2-related factor 2; TGF-β₁: transforming growth factor β1.

gene (β-actin), and each sample was analysed in technical triplicate. Primers used in RT-qPCR are listed in Table 1.

2.11. Immunofluorescence assay

Kidney cryosections at 3 μm thickness were fixed for 15 min in 4% paraformaldehyde, followed by permeabilisation with 0.5% Triton for 5 min at room temperature. After blocking with 2% donkey serum for 60 min, the slides were immunostained with anti-fibronectin (GB114491, Serviocebio, Wuhan, China), anti-collagen I (GB114197, Serviocebio, Wuhan, China), anti-collagen III (GB111629, Serviocebio, Wuhan, China) and anti-nuclear factor erythroid 2-related factor 2 (Nrf2) (AF0639, Affinity, Changzhou, China) overnight, followed by incubation with rhodamine-labelled goat anti-rabbit IgG (GB112199, Serviocebio, Wuhan, China) and a green fluorescent protein secondary antibody (GB21303, Serviocebio, Wuhan, China) for 1 h at 3℃. Then, 1× PBS was used to wash the slides three times, and the slides were incubated with 5 μg/mL 40,6-diamidino-2-phenylindole solution for 5 min in the dark and then washed five times. Then, an anti-fluorescence quenching agent was used to seal each slide. Sections were scanned by an optical microscope and quantified using Image J software.

2.12. Western blotting (WB)

Total protein of kidney tissue was obtained by a lysis buffer (R0010, Solarbio, Beijing, China) with protease inhibitor (MB2678-1, Meilunbio, Dalian, China) and phosphatase inhibitor cocktail (MB12707-1, Meilunbio, Dalian, China). Protein concentrations were measured via bicinchoninic acid (BCA) kit (PC0020, Solarbio, Beijing, China). About 30 μg per sample was separated on 8 or 10% sodium dodecyl sulphate-polyacrylamide (SDS-PAGE) gel, transferred to a polyvinylidene fluoride (PVDF) membrane (IPVH00010, Millipore, USA). The membranes were then blocked with 5% serum albumin/tris buffered saline tween (TBST) solution and incubated with appropriate primary antibodies against β-actin (AM21002, HUABIO, Hangzhou, China), E-cadherin (AF7718, Affinity, Changzhou, China), α-smooth muscle actin (α-SMA) (AF1032, Affinity, Changzhou, China), FTH1 (ET1610-78, HUABIO, Hangzhou, China), GPX4 (ET1706-45, HUABIO, Hangzhou, China), solute carrier family 7 member (SLC7A11) (DF12509, Affinity, Changzhou, China), acyl-CoA

synthetase long-chain family member 4 (ACSL4) (ET711-43, HUABIO, Hangzhou, China), transforming growth factor β1 (TGF-β_1) (AF1027, Affinity, Changzhou, China), phosphorylated Smad2 (ET1612-32, HUABIO, Hangzhou, China), Smad2 (ET1604-22, HUABIO, Hangzhou, China), phosphorylated Smad3 (AF3362, Affinity, Changzhou, China), Smad3 (ET1607-41, HUABIO, Hangzhou, China), Nrf2, kelch-like ECH-associated protein 1 (Keap1) (AF5266, Affinity, Changzhou, China) and haeme oxygenase-1 (HO-1) (AF5393, Affinity, Changzhou, China) overnight at 4°C. After rinsing, the membranes were sequentially hybridised with the corresponding horseradish peroxidase (HRP)-conjugated secondary antibody at room temperature for 1 h. Finally, immunoblots were visualised by the ultra-high sensitivity ECL (HY-K1005, Med Chem Express, USA) and quantified using Image J software.

2.13. Statistical analysis

All quantitative data were expressed as mean ± standard error of the mean (SEM). Statistical analysis were performed with one-way analysis of variance (ANOVA) by GraphPad Prism 8.0 (GraphPad Software, La Jolla, CA). A p-value < 0.05 was considered statistically significant.

3. Results

3.1. Lipus improved renal function and alleviated kidney injury in ADR-Induced CKD rats

To evaluate whether LIPUS can alleviate ADR-induced chronic kidney injury, rats were stimulated with or without LIPUS daily for four weeks (Figure 1(A)). First, dynamic weight monitoring showed that the growth rate of rat weight decreased obviously after two injections of ADR, but daily treatment with LIPUS could reduce this weight loss caused by chemotherapy drug (Figure 1 (B)). As for the renal function, amount of 24 h urinary total protein of the CKD + LIPUS group was significantly lower than that of the CKD group both at the third and last week (Figure 1(C)), which proved that continuous LIPUS treatment could protect kidneys from the early stage of CKD, that is acute kidney injury. The blood biochemical test showed that Scr and BUN of the CKD + LIPUS group were significantly lower than those of the CKD group (Figure 1(D,E)), which once again confirmed that LIPUS could effectively delay the damage of ADR on renal function.

H&E staining showed ADR-induced serious renal histological damage including glomerular dilatation, tubular dilatation, tubular epithelial injury and lumen destruction (Figure 1(F)). According to the histopathological scoring, we found that the damaged degree of nephron in the CKD group was between severe injury and large area injury, and however, it was significantly decreased in the CKD + LIPUS group (Figure 1(G)). In addition, PAS staining showed that more glycogen was accumulated in dilated renal glomeruli and tubules of the CKD group (Figure 1(H)). These suggest that LIPUS treatment significantly improved kidney injury in the ADR-induced CKD model.

3.2. Lipus inhibited renal inflammation in ADR-Induced CKD model

We next investigated the inhibitory effect of LIPUS therapy on renal inflammation because the sustained release of inflammatory mediators is the main reason for the excessive accumulation of extracellular matrix and renal fibrosis [22]. First, RT-qPCR showed that the mRNAs of IL-1β and IL-6 were obviously over-expressed after ADR induction (Figure 2(A,B)). However, LIPUS treatment reduced the mRNA expression level of inflammatory factors (Figure 2(A,B)). Then, we further verified the above results at the protein level by ELISA. Specifically, the protein levels of IL-1β and IL-6 in the Control group and the CKD + LIPUS group were significantly lower than those in the CKD group, and although the histone expression of the CKD + LIPUS was slightly higher than that of the Control group, there was no significant difference (Figure 2(C,D)). Therefore, it is believed that LIPUS can effectively inhibit the persistent renal inflammation caused by ADR.

3.3. Lipus ameliorated renal fibrosis in ADR-Induced CKD model

Renal fibrosis is the most important pathological manifestation in the middle and late stage of CKD, and it is also an important inducement of progressive renal inflammatory reaction [4,22]. Therefore, it was necessary to explain the pathological basis of LIPUS for treating CKD by evaluating the degree of fibrosis in each group. To begin with, ultrasonic elastography was used to evaluate the hardness of living rat kidney. The results showed that ADR had induced renal sclerosis in the CKD group and the CKD + LIPUS group, but LIPUS treatment could reduce the degree of renal sclerosis in rats (Figure 3(A)). At the same time, Mason's trichrome staining and fibrosis quantitative analysis also provided evidence from the micro level to show that the dilated glomerular and renal interstitial space of the CKD group was filled with blue collagen fibres, whereas the CKD + LIPUS group was significantly lower than that of the CKD group (Figure 3(B,C)).

To further confirm the anti-fibrosis effect of LIPUS, the kidney slices were stained with immunofluorescence. The results showed that ADR induced an extensive accumulation of fibronectin in glomeruli, collagen I in renal tubules and collagen III in tubulointerstitial, but the stimulation with LIPUS significantly reduced the content of these collagen fibres (Figure 4(A–D)). In addition, WB (Figure 4(E–G)) and RT-qPCR (Figure 4(H,J)) revealed that the inhibitory effect of LIPUS on collagen fibres was achieved by increasing the E-cadherin expression and decreasing the α-SMA expression. To sum up, the above results strongly suggest that LIPUS could delay the development of renal fibrosis in the ADR-induced CKD rats.

### 3.4. Lipus inhibited ferroptosis in ADR-induced CKD model

Ferroptosis is characterised by the iron-dependent intracellular accumulation of ROS and lipid peroxide products, which could lead to DNA double-strand breaks and positive on TUNEL staining [15,23]. Therefore, we first measured the iron content in kidney tissues and found that iron deposits and Fe^{2+} levels were notably increased in the CKD group when compared with control group (Figure 5(A,D,E)). Nevertheless, LIPUS prominently reduced the accumulation of iron deposits and Fe^{2+} (Figure 5(A,D,E)). WB showed decreased FTH1 expression in the kidneys of the CKD group when compared with the control group, while LIPUS
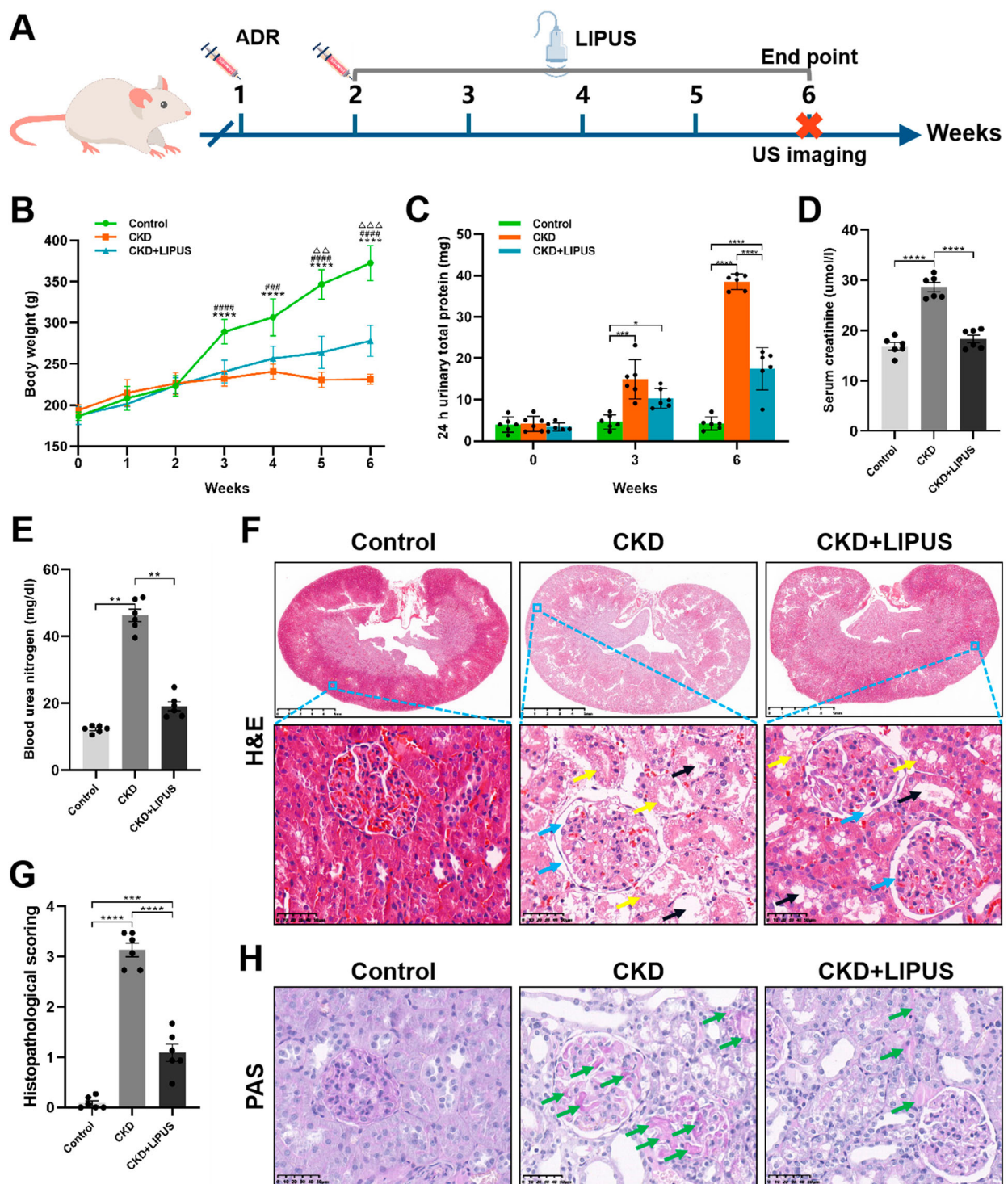
Figure 1. Treatment with LIPUS alleviated the deteriorations of renal function and pathological damage in the ADR-induced CKD rat. (A) A schematic of LIPUS treatment. (B) Changes in body weight overtime (****$p < 0.0001$ vs. the Control/CKD group, ###$p < 0.001$, ####$p < 0.0001$ vs. the CKD/CKD + LIPUS group, △△$p < 0.01$, △△△$p < 0.001$, vs. the Control/CKD + LIPUS group). (C) Changes of 24 h urinary total protein at the 0th, 3rd and 6th weeks. (D, E) Levels of serum creatinine and blood urea nitrogen at the 6th week. (F) Representative micrographs of haematoxylin eosin (H&E) staining in each group. Scale bar, 5 mm/50 μm. Renal histological damage including glomerular dilatation (blue arrows), tubular dilatation (black arrows), tubular epithelial injury and lumen destruction (yellow arrows). (G) Histopathological scoring. (H) Representative micrographs of periodic acid Schiff (PAS) staining in each group. Scale bar, 50 μm. Glycogen was accumulated in dilated renal glomeruli and tubules (green arrows). Data represent the mean ± standard error of the mean (SEM) for 6 rats in each group. *$p < 0.05$, ** $p < 0.01$, ***$p < 0.001$, **** $p < 0.0001$.

treatment increased the expression of FTH1 proteins in the CKD + LIPUS group (Figure 5(B,F)). Additionally, there were significantly more TUNEL-positive cells in the CKD group than the CKD group and the CKD + LIPUS group (Figure 5(C, G)). It is proved that LIPUS treatment does reduce the apoptosis of renal cells induced by ADR. Next, we stained the renal slices with ROS fluorescence. The results showed that the content of ROS in renal tubular epithelial cells (TECs) of the

CKD group was significantly higher than that of the Control group. However, after treatment with LIPUS, the ROS level decreased (Figure 6(A,B)). ELISA confirmed that ADR-induce resulted in a lot of LPO (Figure 6(C)), O_2^- (Figure 6(D)) and MDA (Figure 6(E)) in kidney tissue. Similarly, LIPUS treatment also significantly reduced the levels of these lipid peroxides, and effectively inhibited the lipid peroxidation process in CKD + LIPUS group (Figure 6(C–E)).
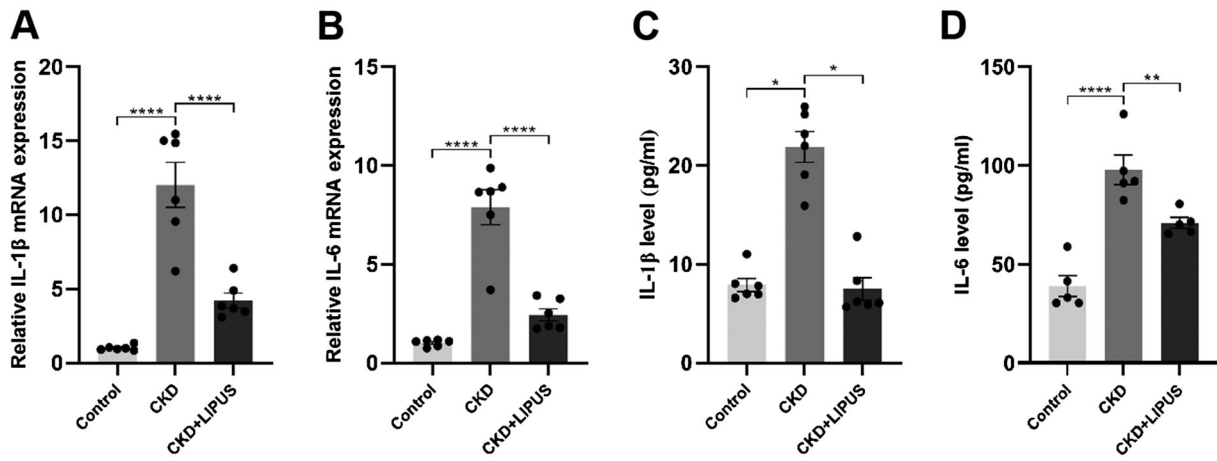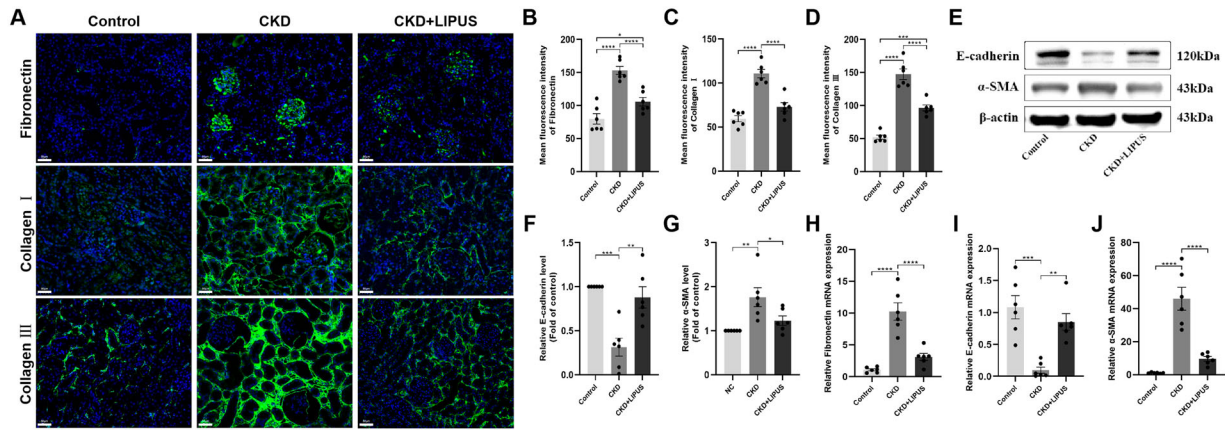
Figure 2. Treatment with LIPUS suppressed the expression of inflammatory factors in the ADR-induced CKD rat. The mRNA expression levels of (A) IL-1β (interleukin-1β) and (B) IL-6 (interleukin-6) in rat kidney tissue were assayed by real-time quantitative polymerase chain reaction (RT-qPCR). (C) The protein expression levels of (C) IL-1β and (D) IL-6 in rat kidney tissue were assayed by enzyme linked immunosorbent assay (ELISA). Data represent the mean ± standard error of the mean (SEM) for 6 rats in each group. *$p < 0.05$, ** $p < 0.01$, **** $p < 0.0001$.

We also evaluated the antioxidant stress system of rat kidney. Both of GPX4 and SLC7A11 are the key biomarkers of ferroptosis and play important roles in anti-oxidative stress [15,23]. WB showed that the protein expression levels of GPX4 (Figure 7(A,B)) and SLC7A11 (Figure 7(A,C)) in the CKD group were significantly lower than those in the control group, but LIPUS treatment reversed this situation to some extent. The expression trend of GPX4 mRNA
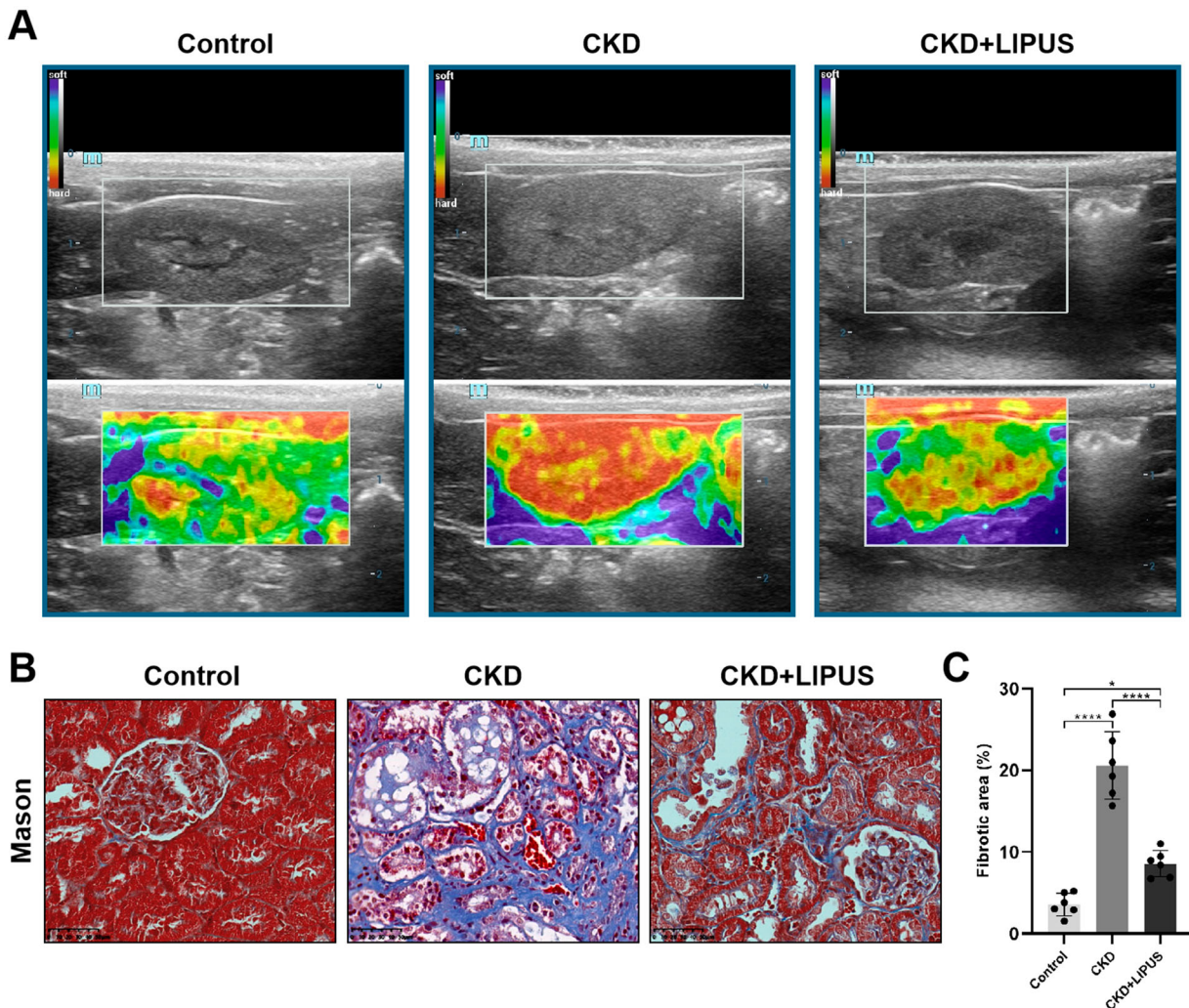
Figure 3. Treatment with LIPUS ameliorated kidney hardness and renal fibrosis in the ADR-induced CKD rat. (A) Representative elastic map of each group on the classical ultrasound image in coronal views. The elastic map is colour-coded from 0 to 45 kPa, with red representing the hardest, yellow representing relatively hard, green representing relatively soft, and blue represents the softest. (B) Representative micrographs of Masson's trichrome staining in each group. Scale bar, 50 μm. (C) Quantification of fibrotic area, expressed as a percentage of the total area. Data represent the mean ± standard error of the mean (SEM) for 6 rats in each group. *$p < 0.05$, **** $p < 0.0001$.

Figure 4. Treatment with LIPUS inhibited the expression of fibrin and fibrosis factor in the ADR-induced CKD rat. (A) The expression levels of fibronectin, collagen I and collagen III in rat kidney tissue were assayed by immunofluorescence. Scale bar, 50 μm. The absolute expression levels of fibronectin (B), collagen I (C) and collagen III (D) were quantified as the average fluorescence intensity. (E) The protein expression levels of E-cadherin and α-smooth muscle actin (α-SMA) in rat kidney tissue were assayed by western blotting (WB). Relative expression levels of E-cadherin (F) and α-SMA (G) in each group. The mRNA expression levels of fibronectin (H), E-cadherin (I) and α-SMA (J) in rat kidney tissue were proved by real-time quantitative polymerase chain reaction (RT-qPCR). Data represent the mean ± standard error of the mean (SEM) for 6 rats in each group. *$p < 0.05$, ** $p < 0.01$, ***$p < 0.001$, **** $p < 0.0001$.

confirmed WB results (Figure 7(E)). Secondly, ACSL4 is an important enzyme in regulating ferroptosis [24]. This study found that ADR-induction significantly increased the protein expression level of ACSL4 in CKD group (Figure 7(A,D)). On the contrary, LIPUS treatment reduced its expression. Furthermore, ELISA also revealed that the redox homeostasis of renal tissue in the CKD group was destroyed, but LIPUS treatment alleviated this injury. Specifically, compared with the control group, ADR-induce inhibited the activities of T-SOD (Figure 7(F)) and decreased the level of GSH (Figure 7(G)) and GSH-Px (Figure 7(H)). These antioxidants were significantly increased in the CKD + LIPUS group with LIPUS treatment (Figure 7(F–H)).

Finally, it is considered that mitochondria are the executors of ferroptosis [23,25]. Therefore, we observed rat TECs with the electron microscope. The ultrastructural analysis demonstrated that ADR induced the distinctive morphological features of the CKD group, involving shrunken mitochondria with increased membrane density and mitochondrial ridge reduction or even disappearance (Figure 7(I)). By contrast, LIPUS treatment strengthened the mitochondrial resistance of TECs (Figure 7(I)).

3.5. LIPUS regulated TGF-β1/Smad and Nrf2/Keap1/HO-1 signalling pathways in ADR-induced CKD model

The TGF-β_1/Smad pathway has long been considered a key signalling pathway for inducing renal fibrosis [10,26]. We investigated whether LIPUS treatment could inhibit TGF-β_1/Smad signalling in the ADR-induced CKD model. First, WB showed that the protein levels of TGF-β_1 (Figure 8 (A,B)), p-Smad2 (Figure 8(C)) and p-Smad3 (Figure 8(A,D)) were significantly increased in the CKD group, while these proteins were decreased in the CKD + LIPUS group after LIPUS treatment (Figure 8(A–D)). The expression trend of TGF-β_1 mRNA was consistent with the WB result (Figure 8 (E)). These findings indicated that LIPUS can effectively improve renal fibrosis in the ADR-induced CKD rat by inhibiting TGF-β_1/Smad pathway (Figure 10).

Nrf2/Keap1/HO-1 pathway could maintain the balance of redox homeostasis by regulating a series of proteins and enzymes [27]. In addition, Nrf2 is also closely related to

cellular iron metabolism [28]. In this study, we found that the ADR-induce dramatically reduced the protein abundance of Nrf2 (Figure 9(A,B)) and HO-1 (Figure 9(A,D)), and simultaneously increased Keap1 (Figure 9(A,C)) expression. Conversely, LIPUS treatment dramatically elevated the protein levels of Nrf2 and HO-1 but decreased Keap1 expression in the CKD + LIPUS group (Figure 9(A–D)). In addition, immunofluorescence showed that LIPUS treatment promoted the accumulation of Nrf2 in the nucleus (Figure 9(E,F)). The expression trend of Nrf2 mRNA was consistent with the WB result (Figure 9(G)). Accordingly, the above results indicated that LIPUS treatment inhibited CKD-related oxidative stress and ferroptosis by regulating Nrf2/Keap1/HO-1 pathway (Figure 10).

4. Discussion

Renal inflammation and fibrosis are the universal pathological features and play a pivotal role in the pathogenesis of CKD [29]. Therefore, inhibiting renal inflammation and renal fibrosis is critical for protecting renal function. Compared with drug therapy and other treatments, continuous physical stimulation in vitro can provide considerable therapeutic effect for CKD patients, and greatly reduce the potential drug toxicity risk and high treatment cost [6]. Encouragingly, some recent experimental studies revealed that LIPUS stimulation with appropriate intensity can provide continuous protection for various animal models of renal injury at different stages [10,11,30,31]. In this study, we further tested the benefits of LIPUS for CKD using the ADR-induced CKD rat model. The results demonstrated that LIPUS stimulation with 60 mW/cm^2 intensity and 50% duty cycle applied to bilateral kidneys of rat every day for four weeks, which could effectively inhibit the ADR-induced renal inflammation, fibrosis and ameliorate renal function as manifested by the decreased levels of urinary albumin, Scr and BUN. Mechanistically, we found that the abnormal iron metabolism and oxidative stress in CKD rats were simultaneously suppressed by LIPUS treatment. This suggested that ferroptosis may be the main type of cell death in ADR-induced renal injury, and it could be inhibited by LIPUS. Finally, our data evidenced that the treatment efficacy of LIPUS in CKD is closely
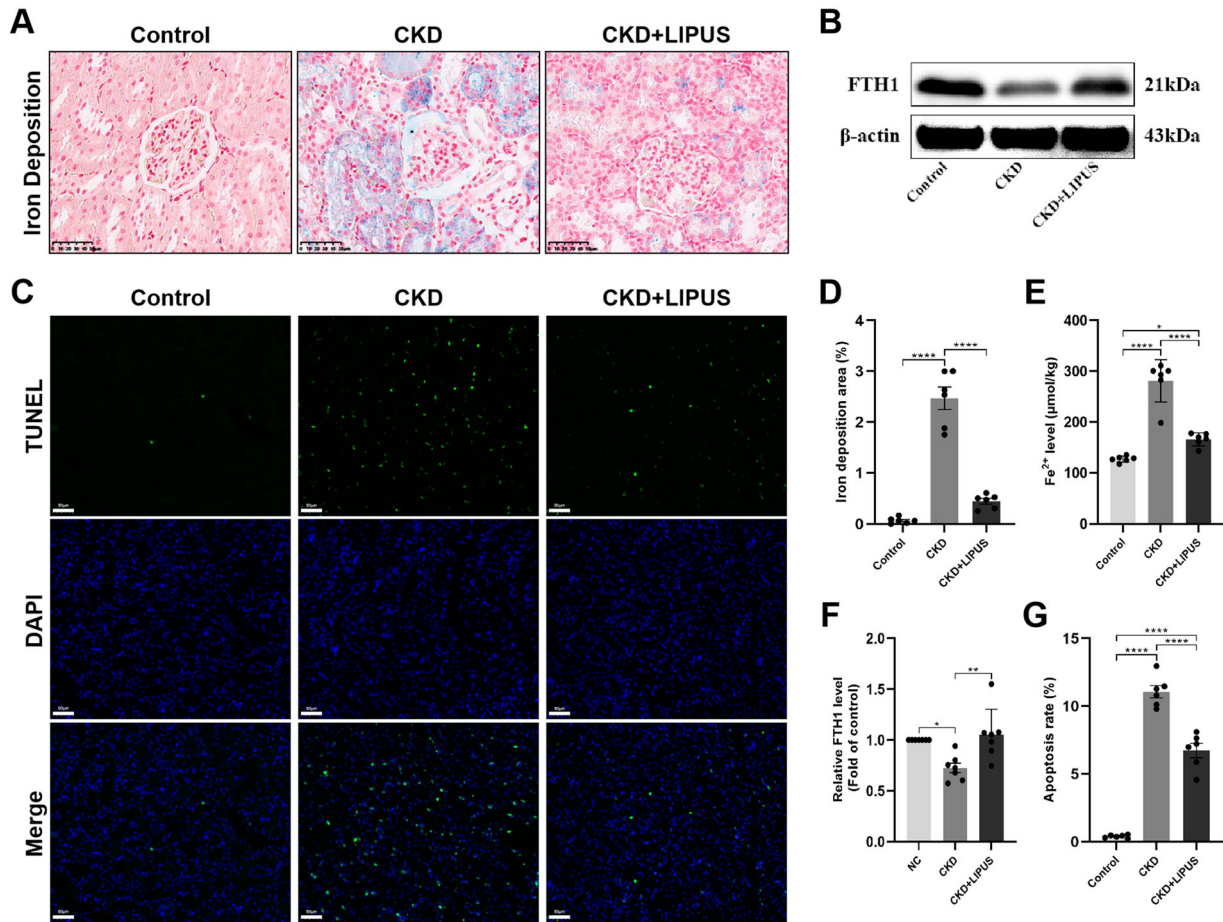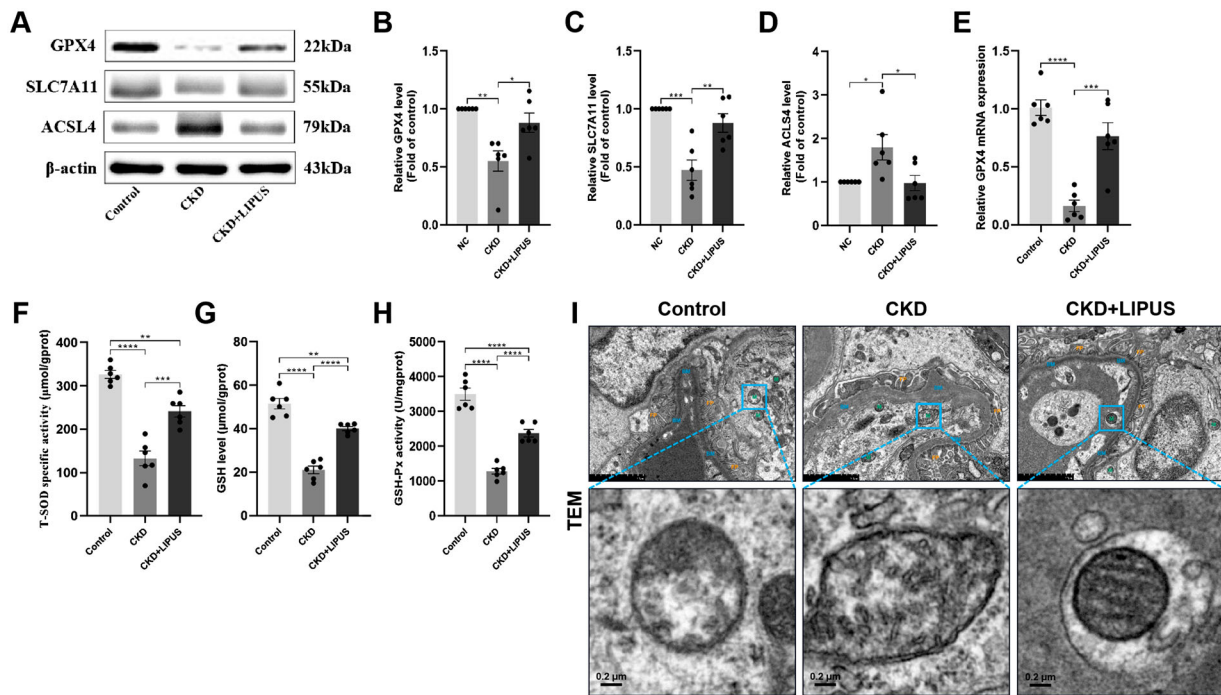
Figure 5. Treatment with LIPUS improved iron deposition and apoptosis in the ADR-induced CKD rat. (A) Representative micrographs of iron staining in each group. Scale bar, 50 μm. (D) Quantification of iron deposition area, expressed as a percentage of the total area. (E) The levels of Fe^{2+} in rat kidney tissue were assayed by enzyme linked immunosorbent assay (ELISA). (B) The protein expression level of ferritin heavy chain 1 (FTH1) in rat kidney tissue was assayed by western blotting (WB). (F) Relative expression levels of FTH1. (C, G) Representative micrographs of TUNEL staining and result of apoptosis analysis in each group. Data represent the mean ± standard error of the mean (SEM) for 6 rats in each group. *$p < 0.05$, ** $p < 0.01$, **** $p < 0.0001$.
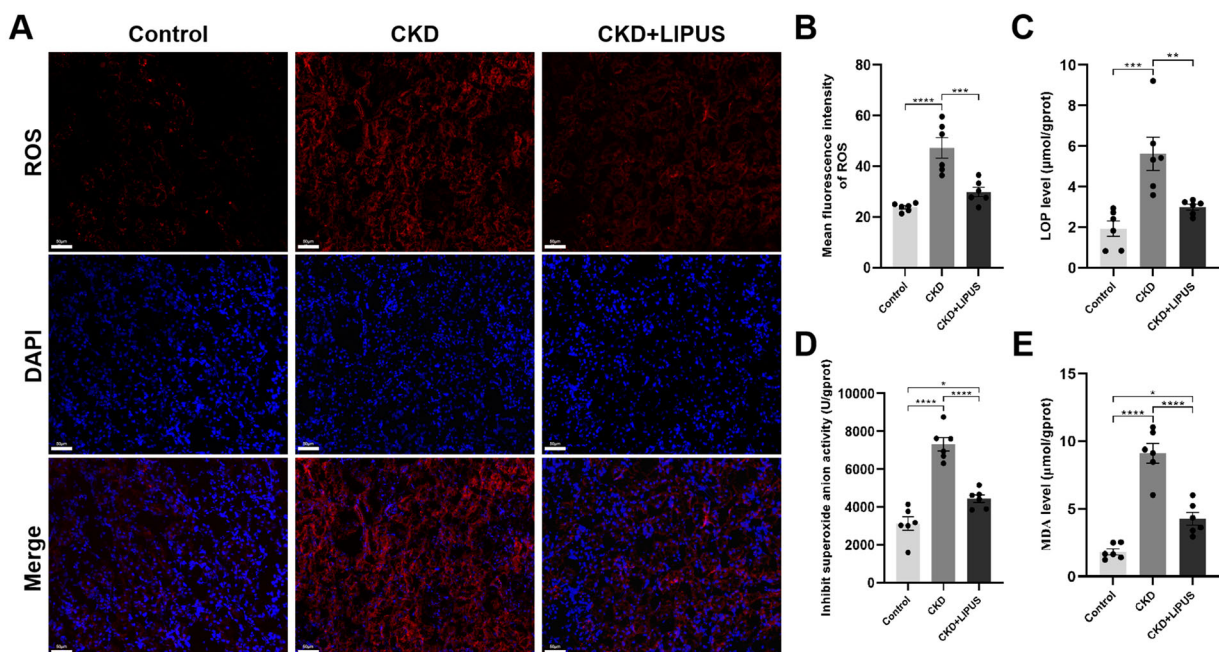
Figure 6. Treatment with LIPUS inhibited ferroptosis-related oxidative stress in the ADR-induced CKD rat. (A) Representative micrographs of reactive oxygen species (ROS) staining in each group. Scale bar, 50 μm. (B) The absolute expression level of ROS was quantified as the average fluorescence intensity. The levels of lipid peroxide (LPO) (C), superoxide anionic (O_2) (D) and malondialdehyde (MDA) (E) in rat kidney tissue were assayed by enzyme linked immunosorbent assay (ELISA). Data represent the mean ± standard error of the mean (SEM) for 6 rats in each group. *$p < 0.05$, ** $p < 0.01$, ***$p < 0.001$, **** $p < 0.0001$.

Figure 7. Treatment with LIPUS strengthened ferroptosis-related antioxidative stress and improved the function of mitochondria in the ADR-induced CKD rat. (A) The protein expression levels of glutathione peroxidase 4 (GPX4), solute carrier family 7 member (SLC7A11) and acyl-CoA synthetase long-chain family member 4 (ACSL4) in rat kidney tissue were assayed by western blotting (WB). Relative expression levels of GPX4 (B), SLC7A11 (C) and ACSL4 (D) in each group. The mRNA expression level of GPX4 (E) in rat kidney tissue were proved by real-time quantitative polymerase chain reaction (RT-qPCR). The levels of total superoxide dismutase (T-SOD) (F), glutathione (GSH) (G) and glutathione peroxidase (GSH-Px) (H) in rat kidney tissue were assayed by enzyme linked immunosorbent assay (ELISA). (I) Ultrastructural alterations of tubular epithelial cells (TECs) were analysed using transmission electron microscopy. scale bar, 2.0μm/0.2μm. Abbreviations: BM, basement membrane; FP, foot process; M, mitochondria. Data represent the mean ± standard error of the mean (SEM) for 6 rats in each group. $*p < 0.05$, $** p < 0.01$, $***p < 0.001$, $**** p < 0.0001$.

related to the regulation of TGF-β_1/Smad and Nrf2/keap1/HO-1 signalling pathways.

To date, LIPUS has been proved to regulate various types of inflammatory reactions and promote tissue repair [6]. In theory, the pulsed acoustic waves emitted by LIPUS contain micro-streaming, which can affect the synthesis and secretion of intracellular protein [32]. It may be the main reason for inhibiting inflammation of cells and tissues. Aibara et al. reported that LIPUS treatment can alleviate the inflammatory injury in hypertensive and diabetic nephropathy mice by inhibiting the infiltration of inflammatory cells and the expression of inflammatory factors such as tumour necrosis factor-α (TNF-α), IL-1β [10]. In our study, within four weeks from the last injection of ADR to euthanasia, IL-1β and IL-6 in kidney tissue increased about two times, but the inflammatory factors, especially IL-1β, decreased significantly after continuous LIPUS treatment. This evidence provides new support for LIPUS to inhibit CKD-related renal inflammation. In addition to the anti-inflammatory effect, we also found that LIPUS treatment down-regulated the expression of α-SMA and E-cadherin, then reduced the abnormal distribution of fibrous protein (fibronectin, collagen I and III) in kidney tissue, and finally significantly alleviated renal fibrosis from pathology. This is consistent with previous studies [10,11]. To sum up, the efficacy of LIPUS in inhibiting renal inflammation and fibrosis is obvious to all in treatment CKD. However, we cannot accurately point to which LIPUS treatment was the key player. It is necessary to explore the underlying logic of LIPUS for treating CKD.
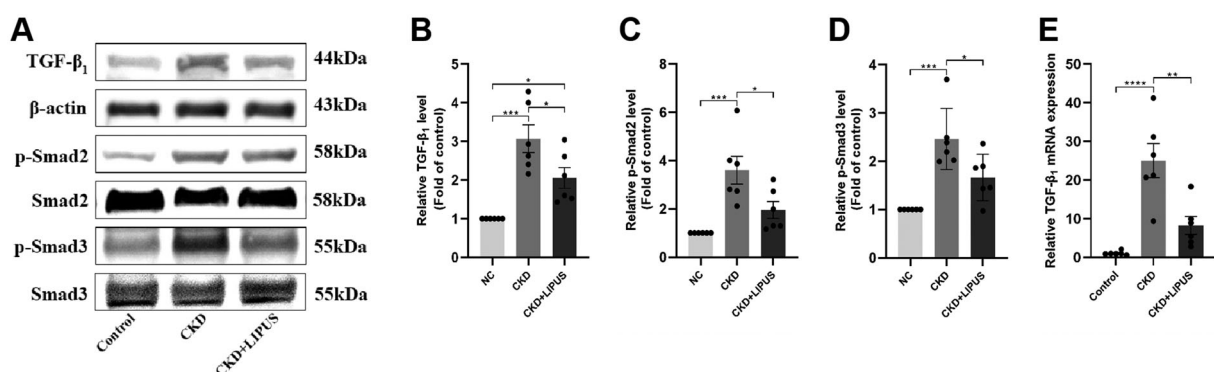

Figure 8. Treatment with LIPUS regulated TGF-β_1/Smad pathway. (A) The protein expression levels of TGF−β_1, phosphorylated Smad2 (p-Smad2) and phosphorylated Smad3 (p-Smad3) in rat kidney tissue were assayed by western blotting (WB). Relative expression levels of TGF−β_1 (B), p-Smad2 (C) and p-Smad3 (D) in each group. The mRNA expression level of TGF−β_1 (E) in rat kidney tissue were proved by real-time quantitative polymerase chain reaction (RT-qPCR). Data represent the mean ± standard error of the mean (SEM) for 6 rats in each group. $*p < 0.05$, $** p < 0.01$, $***p < 0.001$, $**** p < 0.0001$.
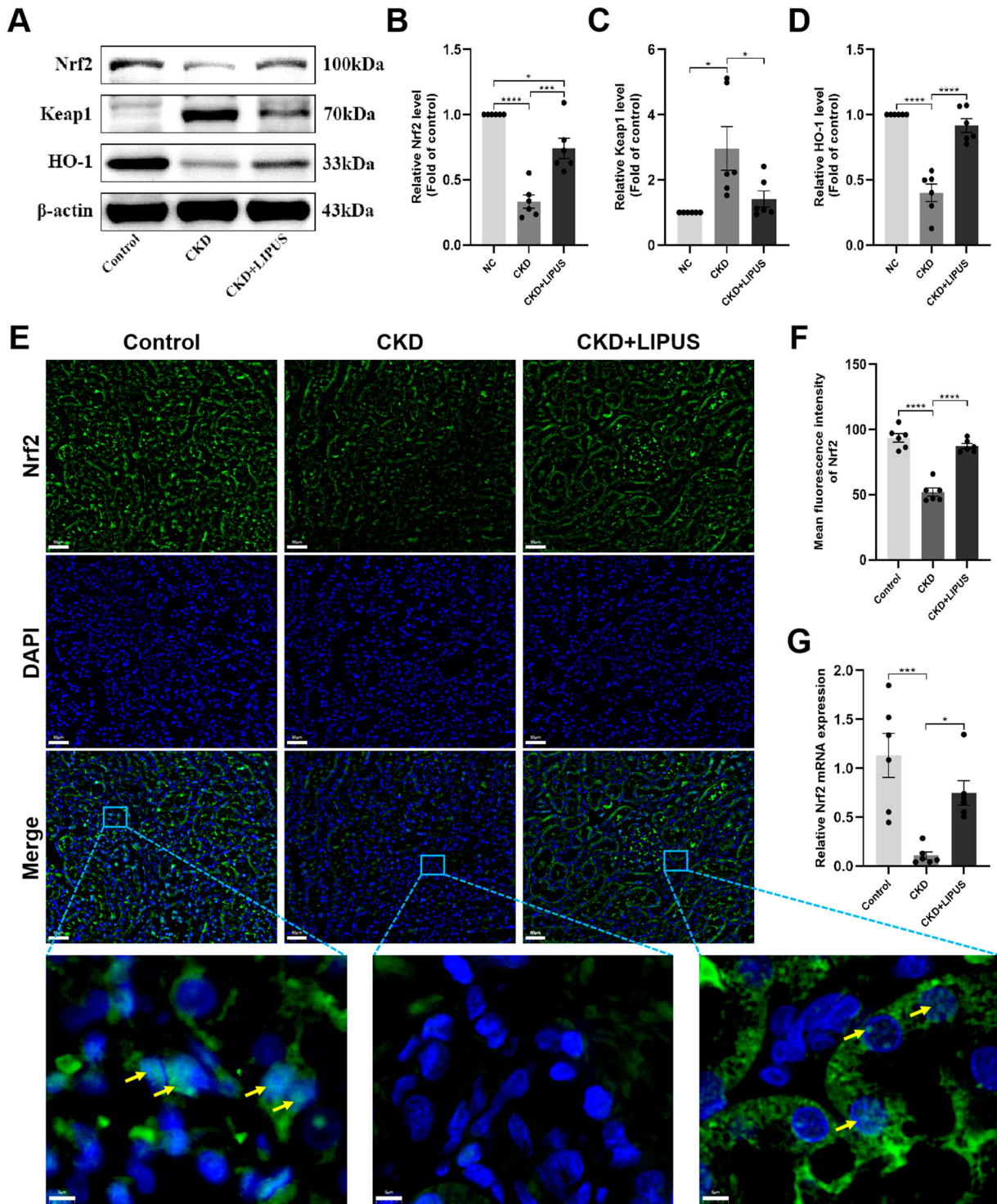
Figure 9. Treatment with LIPUS regulated Nrf2/Keap1/HO-1 signalling pathway by promoting the expression of NRF 2 and nuclear translocation. (A) The protein expression levels of nuclear factor erythroid 2-related factor 2 (Nrf2), kelch-like ECH-associated protein 1 (Keap1) and haeme oxygenase-1 (HO-1) in rat kidney tissue were assayed by western blotting (WB). Relative expression levels of Nrf2 (B), Keap1 (C) and HO-1 (D) in each group. (E) The expression level and nuclear translocation (yellow arrows) of Nrf2 detected by immunofluorescence. Scale bar, 50 μm/5μm. (G) The mRNA expression level of Nrf2 in rat kidney tissue were proved by RT-qPCR. Data represent the mean ± standard error of the mean (SEM) for 6 rats in each group. *$p < 0.05$, ***$p < 0.001$, **** $p < 0.0001$.

Accumulating evidence revealed that ferroptosis is the key player in driving kidney injury rather than other types of cell death [33–35]. Abnormal metabolism and massive accumulation of iron in tissues and organs is one of the most important causes of ferroptosis. In this study, we found that a large amount of iron deposits appeared in the renal parenchyma of ADR-induced CKD rats with the level of Fe^{2+} increasing about two times. At the same time, FTH1 expression decreased significantly. This was consistent with the result of Shao et al. [36]. Interestingly, after undergoing continuous LIPUS stimulation,

the abnormal accumulation of iron in rat kidney were obviously alleviated. It may be attributed to LIPUS treatment reversing the exhaustion of FTH1 protein. Because FTH1 can catalyse the conversion of ferrous iron to the ferric iron by its oxidase activity, and promote iron to be incorporated into ferritin, thereby sequestrating and storing free iron in a non-toxic and bioavailable form [37]. The above evidence preliminary showed that ADR induced abnormal metabolism and distribution of iron in rat kidney, and however, it could be regulated by LIPUS treatment.
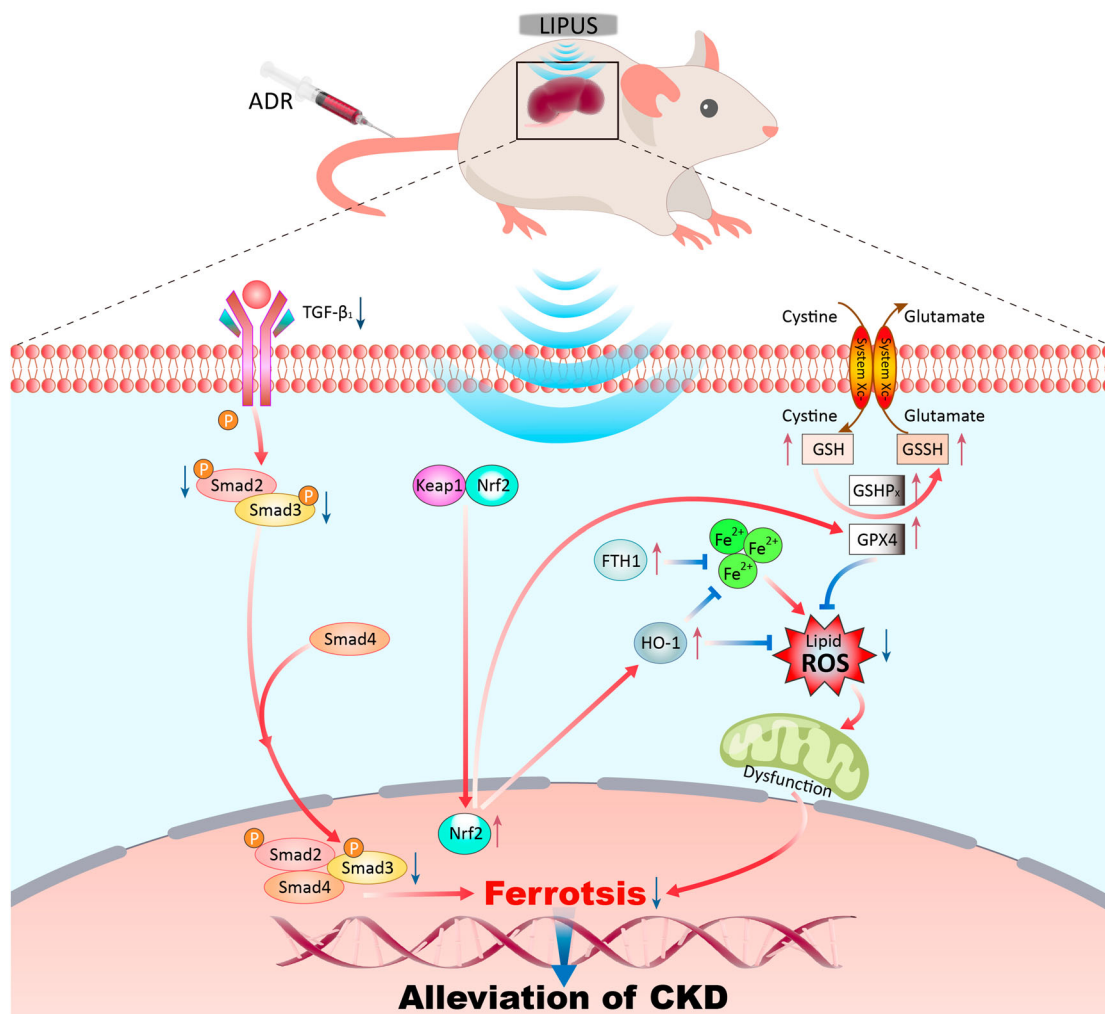
Figure 10. Schematic diagram of LIPUS treating CKD by inhibiting ferroptosis through regulating the TGF-β₁/Smad and the Nrf2/Keap1/HO-1 signalling pathway

Oxidative stress is the central link leading to ferroptosis and is synchronously regulated by oxidative stress system and redox system [35]. On the one hand, with the disruption of iron uptake, storage, and excretion homeostasis, excessive free Fe^{2+} in kidney will produce a lot of ROS through the Fenton reaction ($Fe^{2+} + H_2O_2 \rightarrow Fe^{3+} + OH\text{-} + \cdot OH$) [23,38]. When ROS meets phospholipid-rich biofilm, it will lead to lipid peroxidation, and MDA, which is easy to form adducts with proteins and DNA, resulting in significant cytotoxicity and ferroptosis [35,39]. On the other hand, while redox system will be activated to resist oxidative stress in kidney. The GPX4, an antioxidant enzyme and a central blocker of ferroptosis, is the only glutathione peroxidase that uses GSH as a co-substrate to reduce phospholipid hydroperoxides to hydroxy phospholipid in the membranes [40]. System Xc− mediates the exchange of Glutamate (Glu) and cystine (Cys) across the plasma membrane, ultimately favouring reduced GSH synthesis [41]. And the role of GSH is to activate GPX4 to eliminate excessive ROS maintain intracellular redox homeostasis and inhibit ferroptosis [23]. Some previous studies revealed that oxidative stress is present from the early stages of CKD and continues to increase as kidney function deteriorates due to antioxidant consumption and increased ROS production [42–44]. Thus, it is believed that ferroptosis may be the root cause of renal inflammation, fibrosis and function injury in CKD.

The present study discovered that based on the background of renal inflammation, fibrosis and function injury, the oxidative stress related to abnormal iron metabolism was upregulated in the kidneys of the CKD rat model induced with ADR, which was characterised by remarkable increases in the ROS, LPO, O₂- and MDA. At the same time, GPX4, SLC7A11, GSH, GSH-Px and T-SOD decreased, which indicated that the redox homeostasis was damaged. In addition, the ACSL4, an enzyme that induces ferroptosis, is also over expressed in the kidneys of CKD rats. The shrunken mitochondria with increased membrane density and the reduced or even disappeared mitochondrial ridge were observed in the kidneys of CKD rats. It is defined as the specific morphological changes of ferroptosis, which were different from other death modes [35]. These conditions improved after LIPUS treatment. Specifically, compared with ADR-induced CKD rats, the products related to oxidative stress and lipid peroxidation such as ROS, LPO, O₂- and MDA decreased significantly in rat kidneys after LIPUS treatment, while the key enzymes in charge of redox system including GPX4 and SLC7A11increased significantly at gene and protein levels. Moreover, the morphology of mitochondria also tends to be normal. These data demonstrated that LIPUS can alleviate renal inflammation and fibrosis by inhibiting ferroptosis, thus protecting renal function in CKD.

In terms of mechanism, we initially detected the classical TGF-β₁/Smad pathway of renal fibrosis. A wide range of animal studies have established TGF-β₁ as the predominant pathogenic factor or 'master regulator' that drives renal fibrosis [45]. In CKD, the active homodimer form of TGF-β₁

binds to TGF-β receptor 2 (TGFR2), which can recruit and activate TGFR1. The active TGFR1 then phosphorylates Smad2 and Smad3, which combine to form a complex and transfer to the nucleus. In nucleus, the p-Smad3 component of the complex binds directly to gene promoters to induce transcription of profibrotic molecules, including α-SMA, fibronectin and collagens, which induce myofibroblast activation and matrix deposition [26,45]. Previous study has confirmed that the efficacy of LIPUS in inhibiting renal fibrosis mainly comes from the regulation of TGF-β$_1$/Smad signalling pathway [10]. Notably, Zhu et al. reported that targeting the interactions of Smad3 and activating transcription factor 3(ATF) can block the signal transduction of ferroptosis pathway, thus inhibiting renal fibrosis in CKD [34]. In this study, we confirmed that LIPUS treatment can block the signal transduction between TGF-β$_1$ and its downstream molecules Smad2 and Smad3, but whether LIPUS affects CKD-related ferroptosis through TGF-β$_1$/Smad pathway synchronously needs further study.

As for the Nrf2/Keap1/HO-1 signalling pathway, which is considered the 'switch' for the endogenous antioxidant system [46]. Under normal conditions, Nrf2 resides in the cytosol bound to its negative regulator Keap1. Keap1 constitutively targets Nrf2 for ubiquitination and proteasomal degradation, thereby maintaining Nrf2 signalling capacity at a low level [27]. When the cells are stimulated with oxidative stress, Nrf2 is activated, separates from Keap1, is trans located from the cytoplasm to the nucleus, and up-regulates the expression HO-1 [47,48]. HO-1 induction could protect the kidney from oxidative stress showing anti-inflammatory and anti-apoptotic activities [49]. In the kidney of ADR-induced CKD rats, we observed a large accumulation of lipid peroxides (such as RSO and MDA), the expression and nuclear translocation of Nrf2 was disrupted, meanwhile the expression of HO-1 was down-regulated. However, after LIPUS treatment, a notable improvement in Nrf2 nuclear translocation was observed. This improvement played a crucial role in rectifying the blocked Nrf2/Keap1/HO-1 signal pathway. As a result, the level of oxidative stress was effectively reduced. It was reported that LIPUS could act as an agonist for Nrf2 and reduce oxidative stress by regulating PI3K-Akt/Nrf2 signalling pathway, thus inhibiting the progress of inflammation in the experimental periodontitis mouse [50]. Additionally, a recent study indicated that up-regulation of Nrf2 could increase the expression of GPX4 and SLC7A11, thus inhibiting diabetes-related ferroptosis and delaying the progress of CKD [35]. Therefore, we suppose that LIPUS treatment can inhibit CKD-related ferroptosis by activating the signal transduction of Nrf2/Keap1/HO-1 pathway to strengthen the redox system, thus preventing the kidney from being injured by oxidative stress and lipid peroxidation. This provides a new direction for further mechanism research.

There were several limitations to the current study. The ADR-induced CKD model is usually accompanied by damage to important organs such as heart and liver except kidney. However, it is still unclear whether LIPUS provided indirect protection for these organs, which is one of our future tasks. In addition, due to the limitation of logistics and resources, there was not a control group without isoflurane anaesthesia in this study. However, the future research should consider including such a control group to further investigate the specific role of isoflurane and distinguish it from the effect of treatment itself.

5. Conclusions

LIPUS treatment could ameliorate kidney function by inhibiting renal inflammation and fibrosis via the regulation of CKD-related ferroptosis. Furthermore, the potential regulation of LIPUS on TGF-β$_1$/Smad and Nrf2/Keap1/HO-1 signalling pathways may be the key to anti-ferroptosis.

Acknowledgements

Disclosure statement

Funding

Availability of data and material

The authors declare that data supporting the findings of this study are available within the article.

ORCID

Cheng-de Liao 🄳 http://orcid.org/0000-0002-8891-7555

References

[1] Global, regional, and national burden of chronic kidney disease, 1990-2017: a systematic analysis for the Global Burden of Disease Study 2017. Lancet. 2020;395(10225):709–733. doi:10.1016/S0140-6736(20)30045-3

[2] Xie Y, Bowe B, Mokdad AH, et al. Analysis of the global burden of disease study highlights the global, regional, and national trends of chronic kidney disease epidemiology from 1990 to 2016. Kidney Int. 2018;94(3):567–581. doi:10.1016/j.kint.2018.04.011

[3] Stenvinkel P, Heimbürger O, Paultre F, et al. Strong association between malnutrition, inflammation, and atherosclerosis in chronic renal failure. Kidney Int. 1999;55(5):1899–1911. doi:10.1046/j.1523-1755.1999.00422.x

[4] Meng XM, Nikolic-Paterson DJ, Lan HY. Inflammatory processes in renal fibrosis. Nat Rev Nephrol. 2014;10(9):493–503. doi:10.1038/nrneph.2014.114

[5] Ying S, Tan M, Feng G, et al. Low-intensity pulsed ultrasound regulates alveolar bone homeostasis in experimental periodontitis by diminishing oxidative stress. Theranostics. 2020;10(21):9789–9807. doi:10.7150/thno.42508

[6] Xu M, Wang L, Wu S, et al. Review on experimental study and clinical application of low- intensity pulsed ultrasound in inflammation. Quant Imaging Med Surg. 2021;11(1):443–462. doi:10.21037/qims-20-680

[7] Liu S, Zhou M, Li J, et al. LIPUS inhibited the expression of inflammatory factors and promoted the osteogenic differentiation capacity of hPDLCs by inhibiting the NF-κB signaling pathway. J Periodontal Res. 2020;55(1):125–140. doi:10.1111/jre.12696

[8] Schandelmaier S, Kaushal A, Lytvyn L, et al. Low intensity pulsed ultrasound for bone healing: systematic review of randomized controlled trials. Br Med J. 2017;356:jj656. doi:10.1136/bmj.j656

[9] Lyu W, Ma Y, Chen S, et al. Flexible ultrasonic patch for accelerating chronic wound healing. Adv Healthc Mater. 2021;10(19):2100785. doi:10.1002/adhm.202100785

[10] Aibara Y, Nakashima A, Kawano KI, et al. Daily Low-intensity pulsed ultrasound ameliorates renal fibrosis and inflammation in experimental hypertensive and diabetic nephropathy. Hypertension. 2020;76(6):1906–1914. doi:10.1161/HYPERTENSIONAHA.120.15237

[11] Lin CY, Wang CC, Loh JZ, et al. Therapeutic ultrasound halts progression of chronic kidney disease In vivo via the regulation of markers associated with renal epithelial-mesenchymal transition and senescence. Int J Mol Sci. 2022;23(21):13387. doi:10.3390/ijms232113387

[12] Tao WH, Shan XS, Zhang JX, et al. Dexmedetomidine attenuates ferroptosis-mediated renal ischemia/reperfusion injury and inflammation by inhibiting ACSL4 via α2-AR. Front Pharmacol. 2022;13:782466. doi:10.3389/fphar.2022.782466

[13] Villalpando-Rodriguez GE, Gibson SB. Reactive oxygen species (ROS) regulates different types of cell death by acting as a rheostat. Oxid Med Cell Longev. 2021;2021:1. doi:10.1155/2021/9912436

[14] Zhuo WQ, Wen Y, Luo HJ, et al. Mechanisms of ferroptosis in chronic kidney disease. Front Mol Biosci. 2022;9:975582. doi:10.3389/fmolb.2022.975582

[15] Dixon SJ, Lemberg KM, Lamprecht MR, et al. Ferroptosis: an iron-dependent form of nonapoptotic cell death. Cell. 2012;149(5):1060–1072. doi:10.1016/j.cell.2012.03.042

[16] Lo YH, Yang SF, Cheng CC, et al. Nobiletin alleviates ferroptosis-associated renal injury, inflammation, and fibrosis in a unilateral ureteral obstruction mouse model. Biomedicines. 2022;10(3):595. doi:10.3390/biomedicines10030595

[17] Li J, Yang J, Zhu B, et al. Tectorigenin protects against unilateral ureteral obstruction by inhibiting Smad3-mediated ferroptosis and fibrosis. Phytother Res. 2022;36(1):475–487. doi:10.1002/ptr.7353

[18] Zhang Q, Hu Y, Hu JE, et al. Sp1-mediated upregulation of Prdx6 expression prevents podocyte injury in diabetic nephropathy via mitigation of oxidative stress and ferroptosis. Life Sci. 2021;278:119529. doi:10.1016/j.lfs.2021.119529

[19] Zhang Y, Mou Y, Zhang J, et al. Therapeutic implications of ferroptosis in renal fibrosis. Front Mol Biosci. 2022;9:890766. doi:10.3389/fmolb.2022.890766

[20] Yildirim D, Bender O, Karagoz ZF, et al. Role of autophagy and evaluation the effects of microRNAs 214, 132, 34c and prorenin receptor in a rat model of focal segmental glomerulosclerosis. Life Sci. 2021;280:119671. doi:10.1016/j.lfs.2021.119671

[21] Serag WM, Barakat N, Elshehabi ME, et al. Renoprotective effect of bone marrow mesenchymal stem cells with hyaluronic acid against Adriamycin- induced kidney fibrosis via inhibition of Wnt/β-catenin pathway. Int J Biol Macromol. 2022;207:741–749. doi:10.1016/j.ijbiomac.2022.03.156

[22] Zeisberg M, Neilson EG. Mechanisms of tubulointerstitial fibrosis. J Am Soc Nephrol. 2010;21(11):1819–1834. doi:10.1681/ASN.2010080793

[23] Wang J, Liu Y, Wang Y, et al. The cross-link between ferroptosis and kidney diseases. Oxid Med Cell Longev. 2021;2021:6654887. doi:10.1155/2021/6654887.

[24] Stockwell BR, Friedmann Angeli JP, Bayir H, et al. Ferroptosis: a regulated cell death nexus linking metabolism, redox biology, and disease. Cell. 2017;171(2):273–285. doi:10.1016/j.cell.2017.09.021

[25] Wang H, Liu C, Zhao Y, et al. Mitochondria regulation in ferroptosis. Eur J Cell Biol. 2020;99(1):151058. doi:10.1016/j.ejcb.2019.151058

[26] Yu XY, Sun Q, Zhang YM, et al. TGF-β/Smad signaling pathway in tubulointerstitial fibrosis. Front Pharmacol. 2022;13:860588. doi:10.3389/fphar.2022.860588

[27] Abdalkader M, Lampinen R, Kanninen KM, et al. Targeting Nrf2 to suppress ferroptosis and mitochondrial dysfunction in neurodegeneration. Front Neurosci. 2018;12:466. doi:10.3389/fnins.2018.00466

[28] Kerins MJ, Ooi A. The roles of NRF2 in modulating cellular iron homeostasis. Antioxid Redox Signal. 2018;29(17):1756–1773. doi:10.1089/ars.2017.7176

[29] Almeida A, Lira R, Oliveira M, et al. Bone marrow-derived mesenchymal stem cells transplantation ameliorates renal injury through anti-fibrotic and anti-inflammatory effects in chronic experimental renovascular disease. Biomed J. 2022;45(4):629–641. doi:10.1016/j.bj.2021.07.009

[30] Chiang CK, Loh JZ, Yang TH, et al. Prevention of acute kidney injury by low intensity pulsed ultrasound via anti-inflammation and anti-apoptosis. Sci Rep. 2020;10(1):14317. doi:10.1038/s41598-020-71330-1

[31] Gouda SAA, Aboulhoda BE, Abdelwahed OM, et al. Low-intensity pulsed ultrasound (LIPUS) switched macrophage into M2 phenotype and mitigated necroptosis and increased HSP 70 in gentamicin-induced nephrotoxicity. Life Sci. 2023;314:121338. doi:10.1016/j.lfs.2022.121338

[32] Carina V, Costa V, Sartori M, et al. Adjuvant biophysical therapies in osteosarcoma. Cancers (Basel). 2019;11(3):348. doi:10.3390/cancers11030348

[33] Zhao Z, Wu J, Xu H, et al. XJB-5-131 inhibited ferroptosis in tubular epithelial cells after ischemia–reperfusion injury. Cell Death Dis. 2020;11(8):629. doi:10.1038/s41419-020-02871-6

[34] Zhu B, Ni Y, Gong Y, et al. Formononetin ameliorates ferroptosis-associated fibrosis in renal tubular epithelial cells and in mice with chronic kidney disease by suppressing the Smad3/ATF3/SLC7A11 signaling. Life Sci. 2023;315:121331. doi:10.1016/j.lfs.2022.121331

[35] Li S, Zheng L, Zhang J, et al. Inhibition of ferroptosis by up-regulating Nrf2 delayed the progression of diabetic nephropathy. Free Radic Biol Med. 2021;162:435–449. doi:10.1016/j.freeradbiomed.2020.10.323

[36] Shao L, Fang Q, Shi C, et al. Bone marrow mesenchymal stem cells inhibit ferroptosis via regulating the Nrf2-keap1/p53 pathway to ameliorate chronic kidney disease injury in the rats. J Recept Signal Transduct Res. 2023;43(1):9–18. doi:10.1080/10799893.2023.2185083

[37] Torti FM, Torti SV. Regulation of ferritin genes and protein. Blood. 2002;99(10):3505–3516. doi:10.1182/blood.V99.10.3505

[38] Koppenol WH. The centennial of the Fenton reaction. Free Radic Biol Med. 1993;15(6):645–651. doi:10.1016/0891-5849(93)90168-T

[39] Ayala A, Muñoz MF, Argüelles S. Lipid peroxidation: production, metabolism, and signaling mechanisms of malondialdehyde and 4-hydroxy-2-nonenal. Oxid Med Cell Longev. 2014;2014:360438. doi:10.1155/2014/360438.

[40] Yang WS, SriRamaratnam R, Welsch ME, et al. Regulation of ferroptotic cancer cell death by GPX4. Cell. 2014;156(1-2):317–331. doi:10.1016/j.cell.2013.12.010

[41] Koppula P, Zhang Y, Zhuang L, et al. Amino acid transporter SLC7A11/xCT at the crossroads of regulating redox homeostasis and nutrient dependency of cancer. Cancer Commun (Lond). 2018;38(1):12. doi:10.1186/s40880-018-0288-x

[42] Sureshbabu A, Ryter SW, Choi ME. Oxidative stress and autophagy: crucial modulators of kidney injury. Redox Biol. 2015;4:208–214. doi:10.1016/j.redox.2015.01.001

[43] Daenen K, Andries A, Mekahli D, et al. Oxidative stress in chronic kidney disease. Pediatr Nephrol. 2019;34(6):975–991. doi:10.1007/s00467-018-4005-4

[44] Duni A, Liakopoulos V, Roumeliotis S, et al. Oxidative stress in the pathogenesis and evolution of chronic kidney disease: untangling Ariadne's thread. Int J Mol Sci. 2019;20(15):3711. doi:10.3390/ijms20153711

[45] Meng XM, Nikolic-Paterson DJ, Lan HY. TGF-β: the master regulator of fibrosis. Nat Rev Nephrol. 2016;12(6):325–338. doi:10.1038/nrneph.2016.48

[46] Cai Y, Xiao R, Zhang Y, et al. Dhpa protects SH-SY5Y cells from oxidative stress-induced apoptosis via mitochondria apoptosis and the Keap1/Nrf2/HO-1 signaling pathway. Antioxidants (Basel). 2022;11(9):1794. doi:10.3390/antiox11091794

[47] Hassanein EHM, Sayed AM, Hussein OE, et al. Coumarins as modulators of the Keap1/Nrf2/ARE signaling pathway. Oxid Med Cell Longev. 2020;2020:1675957. doi:10.1155/2020/1675957.

[48] Ren J, Yuan L, Wang W, et al. Tricetin protects against 6-OHDA-induced neurotoxicity in Parkinson's disease model by activating Nrf2/HO-1 signaling pathway and preventing mitochondria-dependent apoptosis pathway. Toxicol Appl Pharmacol. 2019;378:114617. doi:10.1016/j.taap.2019.114617

[49] El Gheit A, Emam R, N M. Targeting heme oxygenase-1 in early diabetic nephropathy in streptozotocin-induced diabetic rats. Physiol Int. 2016;103(4):413–427. doi:10.1556/2060.103.2016.4.001

[50] Jiang Q, Chen X, Tian X, et al. Tanshinone I inhibits doxorubicin-induced cardiotoxicity by regulating Nrf2 signaling pathway. Phytomedicine. 2022;106:154439. doi:10.1016/j.phymed.2022.154439